ISSN 1070-3632, Russian Journal of General Chemistry, 2014, Vol. 84, No. 11, pp. 2295–2304. © Pleiades Publishing, Ltd., 2014.
Original Russian Text © I.V. Kumpanenko, A.V. Roshchin, N.A. Ivanova, A.V. Bloshenko, N.A. Shalynina, and T. N. Korneeva, 2013, published in Rossiiskii Khimicheskii Zhurnal, 2013, Vol. 57, No. 1, pp. 6–16.

Colorimetry: Choice of Colorimetric Parameters for Chromophore Concentration Measurements

I. V. Kumpanenko, A. V. Roshchin, N. A. Ivanova, A. V. Bloshenko, N. A. Shalynina, and T. N. Korneeva

Semenov Institute of Chemical Physics, Russian Academy of Sciences, ul. Kosygona 4, Moscow, 119991 Russia
e-mail: ivkumpan@chph.ras.ru

Received January 1, 2013

Abstract—The problem of choice of tristimulus color coordinates which uniquely depend on chromophore concentration in an investigated material has been considered. A theoretical study shows that there are no simple analytical formulas for such dependences, and the majority of tristimulus coordinates of various color spaces: *RGB,* CIE (*XYZ*), CIE ($L^*a^*b^*$), CIE ($L^*C^*H^*$), *HSB*, and *CMYK* poorly correlate with the concentration of molecules responsible for color. However, analysis of published papers on this subject provides abundant evidence showing that at least one tristimulus coordinate of the CIE ($L^*a^*b^*$) color space, specifically L^* (lightness), is related to chromophore concentration C by a simple, steadily descending exponential function. The empirical formula $L^* = L^*(C)$ can be successfully applied for instrumental treatment of experimental colorimetric data for the determination of chromophore concentrations.

DOI: 10.1134/S1070363214110498

INTRODUCTION

The development of technologies for monitoring and predicting the state of the environment, specifically hydrosphere, as well as for quality assessment of food products with aim to ensure protection and human health and vital functions and safe operation of potentially hazardous industries envisions suggests development of new, improved approaches to analysis of hazardous chemicals in various matrices.

One of such approaches dials with multichannel methods for detection and quantitation of hazardous chemical substances, i.e. methods which allow concurrent detection of and processing of data for all analytes. As applied to aqueous media, such methods can be based on the use of sensors responding to changes in analyte concentrations. Such devices should be highly sensitive, highly selective, and fast operating.

Indicator test forms which represent chromogenic reagents changing color as a response to chemical reaction can be used as sensor detectors [1]. The most widely used test forms are supports having developed surfaces (paper, powders, tablets, foam and fiber polymers, etc.) and bearing immobilized chromogenic reagents.

Determination of pollutant concentrations in aqueous media using such test forms usually involves comparison of the color developed as a result of chemical reaction with reference colors on the color chart. Comparison can be performed visually, which is presently the most common approach. The best-fit reference color is chosen, and its number in the list gives the analyte concentrations. Clearly, the visual procedure for measuring the color characteristics of reacted test forms cannot satisfy modern requirements. An automated instrumental approach to processing colorimetry data, based on digitalization of color characteristics, should be developed.

Multichannel parallel detection in such an instrumental chemical analysis can be provided if test forms each specific for a particular analyte are arranged as a matrix in a test slide (Fig. 1) [2].

The matrix construction of multichannel sensors allows automation of the procedure of simultaneous injection into test forms of dosed portions of a solution to be analyzed. Due to the chemical reactions that occur simultaneously in all test forms of the test slide, the test forms change color; after the chemical reactions are complete, using, one can, suitable physical detection method and software simultaneously digitalize and

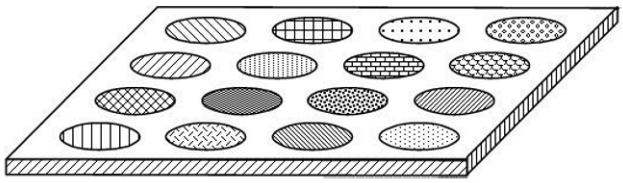

Fig. 1. Design of a matrix test slide containing 16 test forms.

then process primary colorimetry data. In this case, an issue of key importance is to choose color parameters directly related to chromophore concentrations in test forms.

The present paper is devoted to comparative analysis of existing methods of processing colorimetry data and selecting the color space coordinate directly related to the concentration of chromophores in various media (test form, solution, etc.). A great number of published examples are used to illustrate the use as such a coordinate the color lightness L^*, a parameter that is directly related to chromophore concentration. The colorimetric and spectral characteristics of a series of objects (beer, olive oil, vine, pigmented human skin, test forms after completion of color reactions) were compared with the concentrations of components which endow the objects with one or another color.

Relation between Spectral and Colorimetric Parameters

There are two approaches to measure the color characteristics of physical objects: optical spectroscopy in the visible range and colorimetry. In the first case, irradiating light absorption (transmission, reflection) is analyzed as a function of light wavelength (frequency). Spectral data are objective and independent on their perception by a subject (observer). Colorimetry assesses the color of physical objects via visual perception.

The spectral and colorimetric approaches differ from each other, but they are fundamentally interrelated.

According to the three-component theory of color vision, any color is a sum of three components, the so-called basic colors. Any three colors can be treated as basic colors, provided no one of which is impossible to form of the two other ones. There are fairly many sets of three colors, which can form a system of tristimulus color coordinates. The most widespread of them is the *RGB* system with red, green, and blue as basic colors. The following wavelengths correspond to these colors: 700, 546.1, and 435.8 nm. The sum of these colors in a certain ratio gives the most part of almost all existing colors. This system, along with other ones, is presently used in office machines (printers, scanners, monitors) and software (word and image processors).

One of the disadvantages of the *RGB* system is the presence of negative components in the combinations of basic colors for certain real colors (other disadvantages of this system will be discussed below.)

In view of that, in 1931 the International Commission on Illumination (Commission Internationale de l'Eclairage, CIE) developed a standard and proposed a model to describe colors in other color spaces: (*XYZ*), ($L^*a^*b^*$), and ($L^*C^*H^*$).

To understand the physical meaning of these color spaces and be clear about their advantages, let us consider how tristimulus coordinates are calculated in one of them: (*XYZ*).

For color observation one should have three components: (1) light source (illuminant), (2) illuminated object, and (3) observer.

According to the CIE standard, light sources are divided into three types: (*A*) tungsten incandescent lamps with the correlated color temperature 2856 K; (D_{65}) natural day light with the correlated color temperature 6500 K; and (F_{11}) narrow-band white fluorescent lamp with the correlated color temperature 4000 K. The spectra of these light sources, specifically, dependences of radiation intensity on wavelength $S(\lambda)$ are standardized and presented in the digital form in the Russian State Standard GOST R 52489-2005. Figure 2 gives an example of the spectrum of a source of natural day light D_{65}, reconstructed using these data.

An illuminated object is characterized by the diffuse reflection spectrum which is the dependence of diffuse reflection coefficient on wavelength $R(\lambda)$. The diffuse reflection spectrum is an individual characteristic of an object and is measured on a standard spectrometer. As an example, we show in Fig. 3 the diffuse reflection spectra of the reaction products of terminal toluidine groups of foam polyurethane, which are chromogenic agents with the following analytes: 4-nitrophenyldiazonium tetrafluoroborate, active chlorine, and formaldehyde [3]. As seen from the figure, color reactions are accompanied by essential changes in the spectra, and, consequently, in the color of the samples, which can be used as a basis to develop a method for detection and quantitation of analytes in aqueous solutions.

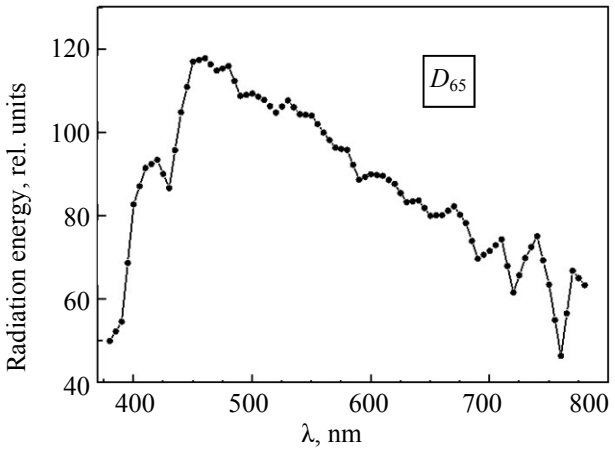

Fig. 2. Emission spectrum of the CIE standard illuminant D_{65}.

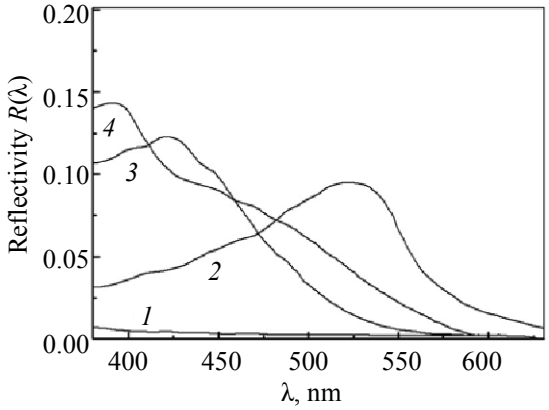

Fig. 3. Diffuse reflection spectra of the (*1*) starting foam polyurethane and (*2*) reaction products of its terminal toluidine groups with (*2*) 4-nitrophenyldiazonium tetrafluoroborate, (*3*) formaldehyde, and (*4*) active chlorine.

The CIE in 1931 introduced the term "standard observer." This term is based on the concept of observer metamerism, i.e. on the fact that color perception is specific of each individual. The standard observer represents a human with an average chromatic response over the entire range of visible light. The color perception of a standard observer depends on the vision angle and is characterized by a set of tristimulus color coordinates: $\bar{x}(\lambda)$ $\bar{y}(\lambda)$ $\bar{z}(\lambda)$. The tristimulus color coordinates for a 10° field-observer, as well as the spectra of illuminants were standardized and implemented in GOST R 52489-2005. The dependences of tristimulus coordinates from wave-length, constructed using these data, are shown in Fig. 4.

Having measured the visible reflection spectrum of an object $R(\lambda)$, one can calculate the color of the object using the radiation spectrum of a standard illuminant $S(\lambda)$ and the wavelength dependences of specific tristimulus coordinates $\bar{x}(\lambda)$ $\bar{y}(\lambda)$ $\bar{z}(\lambda)$. To this end, one calculates the sum of products of the mentioned functions, which give the coordinates of the object in the three-dimensional CIE (*XYZ*) color space:

$$X = k\sum_{\lambda} S(\lambda)\bar{x}(\lambda)R(\lambda)\Delta\lambda,$$

$$Y = k\sum_{\lambda} S(\lambda)\bar{y}(\lambda)R(\lambda)\Delta\lambda,$$

$$Z = k\sum_{\lambda} S(\lambda)\bar{z}(\lambda)R(\lambda)\Delta\lambda, \qquad (1)$$

where

$$k = \frac{100}{\sum_{\lambda} S(\lambda)\bar{y}(\lambda)\Delta\lambda}$$

is the normalizing factor and $\Delta\lambda$, wavelength scale interval (usually 5 nm).

Schematic representation of such calculation is shown in Fig. 5.

The (*XYZ*) color space is not quite convenient in terms of visual color perception, because not all points in the (*XYZ*) space correspond to real color characteristics in view of the nonorthogonality of color-matching functions. Therefore, in practice, the most common spaces are (*RGB*), ($L^*a^*b^*$), (*HSB*), (*CMYK*). The ($L^*a^*b^*$) space is found to be the most useful for concentration measurements, because it makes it possible to differentiate the independent brightness

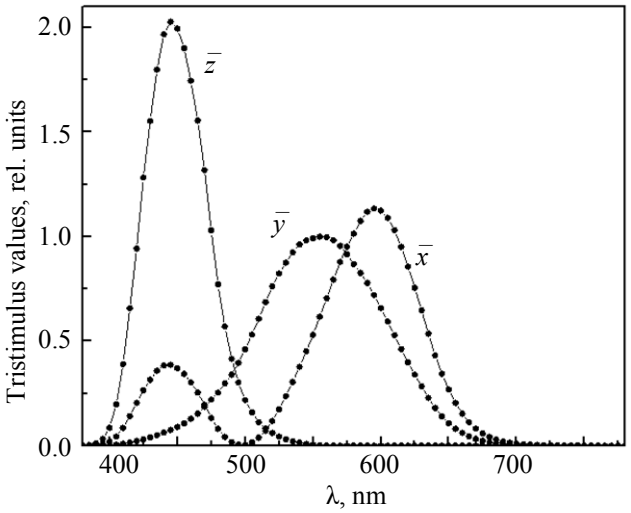

Fig. 4. Dependences of specific tristimulus values for a standard observer on wavelength.

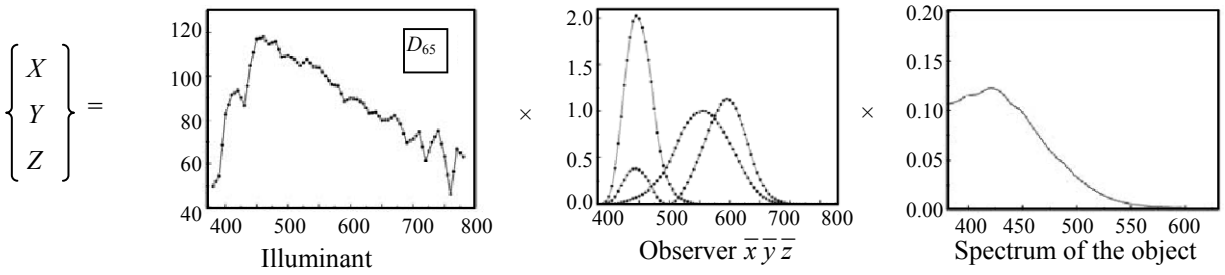

Fig. 5. Schematic representation of the calculations of the (*XYZ*) color coordinates of the reaction products of terminal toluidine groups of foam polyurethane with formaldehyde for the CIE standard illuminant D_{65}.

component (lightness) from color components of the analytical signal.

In the ($L^*a^*b^*$) color space, the lightness of an object is set by the coordinate L^* which varies from 0 to 100, i.e. from the darkest (black) to lightest (white) color, and the chromaticity component is set by two Cartesian coordinates a^* and b^*, each varying from –128 to +127. The first coordinate relates to the color ranging from green to purple, while the second, from blue to yellow.

The transfer from the (*XYZ*) space to ($L^*a^*b^*$) is performed by the following transformation:

$$L^* = 116(Y/Y_n)^{1/3} - 16,$$
$$a^* = 500[(X/X_n)^{1/3} - (Y/Y_n)^{1/3}],$$
$$b^* = 200[(Y/Y_n)^{1/3} - (Z/Z_n)^{1/3}], \quad (2)$$

where X_n, Y_n, Z_n are the coordinates of white light in the (*XYZ*) space.

Below we present some published data to illustrate that the lightness L^* is uniquely dependent on the concentration of the chromophore in a sample.

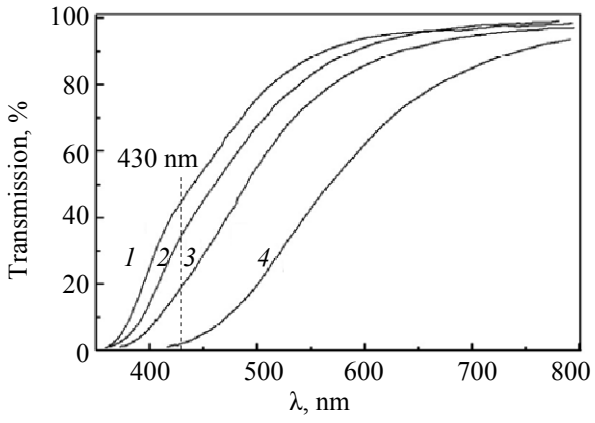

Fig. 6. Visible transmission spectra of European beers: (*1*) M; (*2*) D; (*3*) R; and (*4*) U (M, D, R, and U are beer codes).

Example Uses of Colorimetric and Spectral Data for Determination of Chromophore Concentrations in Colored Objects

Determination of Beer Color by the SRM Color Chart

Analysis of the color of beer for its quality assessment is one of the most illustrative examples of practical colorimetry.

The color of beer depends on its recipe, technology of production, and coloring agents, mainly melanoidines and caramel added to malt. The color of beer is directly related to its visible optical spectrum. Figure 6 shows the spectra of some European beers, measured in the range 350–800 nm. As seen, light transmission falls along the series M > D > R > U over the entire wavelength range; in other words, in going from M to U the beer is getting darker. This is explained by increasing content of chromophores in the beer. Note that the optical spectra of almost all sorts of beer have the characteristic pattern of a steadily rising light transmission–wavelength curve. This circumstance allowed the European Beer Convention (EBC) and American Society of Brewing Chemists (ASBC) to introduce the EBC and SRM (Standard Reference Method) beer color charts based on the measurement of optical density at a single wavelength.

The EBC chart is defined as follows: EBC = $25A_{430}$, where A_{430} is the optical density of the beer spectrum at the wavelength 430 nm, measured in a 1-cm cell.

The SRM chart is related to the EBC chart by the equation:

$$\text{SRM} = 0.508 \cdot \text{EBC}.$$

The versions of the SRM charts, developed by certain European and American firms for different sorts of beers, look like differently colored figures (squares, rectangles, images of wine glasses, etc.), each with its assigned SRM value [4–8] (the versions of the SRM charts).

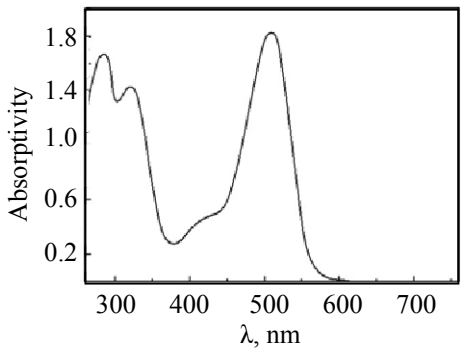

Fig. 7. UV–vis absorption spectrum of acryl derivatives of pelargonidin-3-sophoroside-5-glucoside [12].

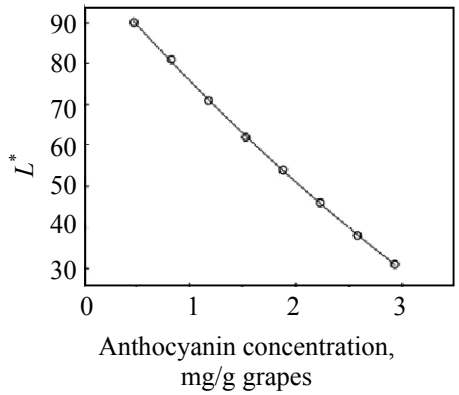

Fig. 8. Dependence of the lightness of grapes L^* on anthocyanin concentration.

The SRM chart provides an approximate and simplified characteristic of color, because it is based on the optical density measured at a single wavelength (430 nm). In this connection of interest is to relate SRM values to lightness L^*. The latter parameter is calculated by the entire visible light spectrum, and, consequently, gives a more adequate characteristic of color.

The L^*values required to construct the L^*–SRM function were determined by the decomposition of an element color of an SRM standard into $L^*a^*b^*$ components or direct transformation of *RGB* coordinates into $L^*a^*b^*$.

The resulting dependences of the beer color lightness L^* on the SRM parameters are illustrated here by the L^*–SRM dependence for beers of various brands [9]. As seen, the three depen-dences corresponding to the *a, b,* and *d* standards are virtually coincident, whereas the dependences for the *c* and *e* standards differ from the three first ones. Moreover, the points on the dependences for real samples show a considerable scatter and much deviate from the curves for the standards.

The coincidence of the curve patterns for three different color standards taken from different sources [4, 5, 7] provides strong evidence for the correctness of these standards. In any case, the L^* values obtained in [9] seem to be overestimated irrespective of the SRM standard.

To summarize the above speculations concerning the beer color estimated by the SRM scale, we would like to note that the L^*–SRM value dependence is unique and monotonic, and, in its turn, the latter parameter is linearly related to the concentration of chromophores in beer. Therefore, the color coordinate L^* can be used for concentration measurements of colored substances.

Determination of Pigment Concentrations in Grapes and Red Wines

The color of grapes and red wines is much dependent on the concentration of the water-soluble pigments anthocyanins, in particular, malvidin-3-glucoside. The color chart for grapes grown in different regions of Australia in different seasons (2005/06, 2006/07, 2007/08) and the corresponding anthocyanin levels in these grapes are reported in [10].

Figure 7 shows typical UV–vis spectra of anthocyanins (acryl derivatives of pelargonidin-3-sophoroside-5-glucoside) [12].

Using the color chart of grapes and the spectrum in Fig. 7, we determined the lightnesses L^* of grapes and constructed a dependence of L^* on anthocyanine concentration (Fig. 8). The dependence is close to linear and described by a descending exponent.

Figure 9 shows the optical spectra of red and white wines of different brands in the range 200–1000 nm [13]. White wines absorb exclusively in the UV range (below 400 nm), whereas red wines both in the UV and visible ranges. Comparison with the spectrum in Fig. 7 allows us to conclude that the visible absorption of red wines is associated with anthocyanins which absorb at 400–600 nm.

To characterize the color depth of a red wine, winemakers commonly use an empirical parameter defined as the sum of absorptivities at three wavelengths (420, 520, and 620 nm), which is called the wine color density (WCD):

$$\mathrm{WCD} = A_{420} + A_{520} + A_{620}.$$

From this equation it follows that the wine color density is proportional to the concentration of anthocyanins.

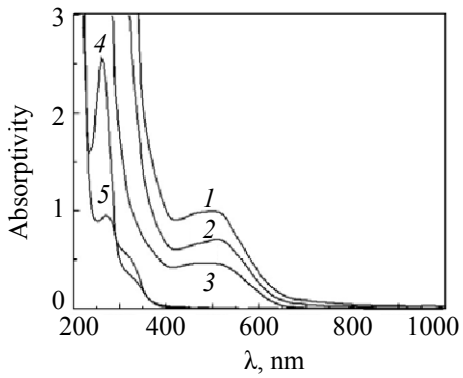

Fig. 9. Absorption spectra of red and white wines: (*1*, *2*, *3*) red wines and (*4*, *5*) white wines.

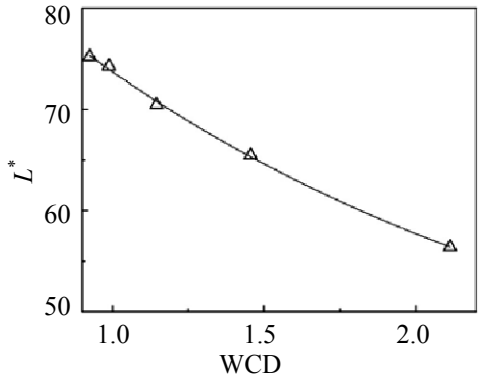

Fig. 10. Dependence of the color lightness L^* of a red wine on its color density (by data in [13])

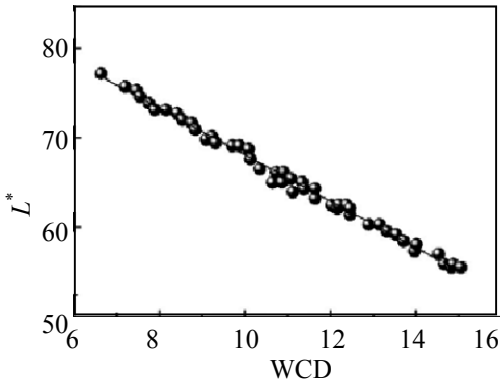

Fig. 11. Linear approximation of the L^*–WCD dependence for Australian wines.

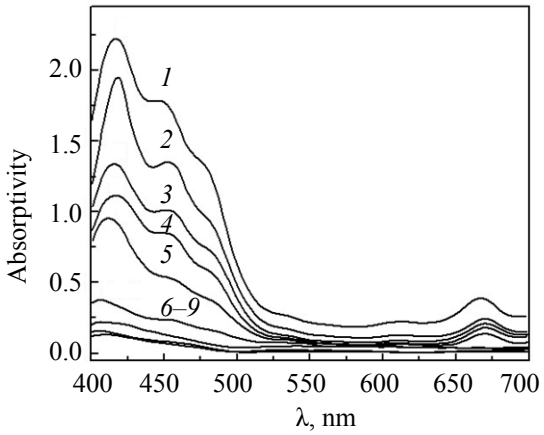

Fig. 12. Visible absorption spectra of olive and colza oils of different brands: (*1*) L EVOO (50%); (*2*) F EVOO; (*3*) C (mixture); (*4*) I EVOO; (*5*) H EVOO; (*6*) D mild; (*7*) K EVOO; (*8*) A canola rapeseed oil; and (*9*) B canola rapeseed oil [14]. (EVOO) Extra Virgin Olive Oil and (A–F, H, K, L) oil producer's codes.

Using the data in Table 1 [13], we constructed a dependence of color lightness L^* on color density for red wines (Fig. 10). As would be expected from a comparison with Fig. 8, this dependence is close to linear and described by a descending exponent.

Table 1. Absorptivities and color densities and lightnesses of red wines

Sample no.	A_{420}	A_{520}	A_{620}	WCD	L^*
1	0.894	0.969	0.250	2.113	56.392
2	0.597	0.695	0.164	1.456	65.478
3	0.428	0.456	0105	0.989	74.303
…	…	…	…	…	…
6	0.460	0.554	0.132	1.146	70.463
7	0.373	0.463	0.089	0.925	75.233

The example of several tens of samples of red wines produced from Sira grapes grown in different regions of Australia in different seasons [11] was used to show that the color lightness L^*–color density dependence is approximated by a straight line (Fig. 11). The above evidence suggests that L^*–chromophore concentration dependences are well fitted by steadily descending functions.

Evaluation of Olive Oil Color

The color of olive oil depends on the concentrations of two its pigments: chlorophylls and carotenoids. Chlorophylls adsorb in the blue and red ranges of the visible light and have a green color. Carotenoids absorb in the blue range and are colored yellow, orange, and red.

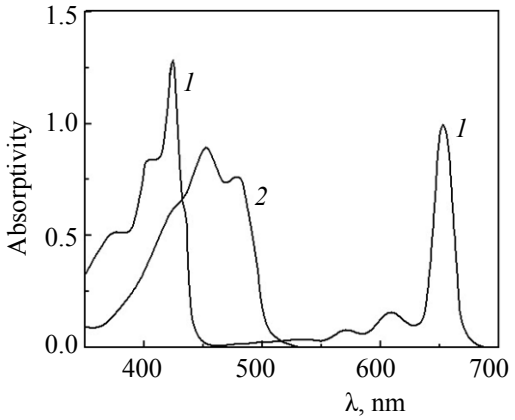

Fig. 13. Absorption spectra of (*1*) chlorophyll *a* and (2) β-carotenoid [15].

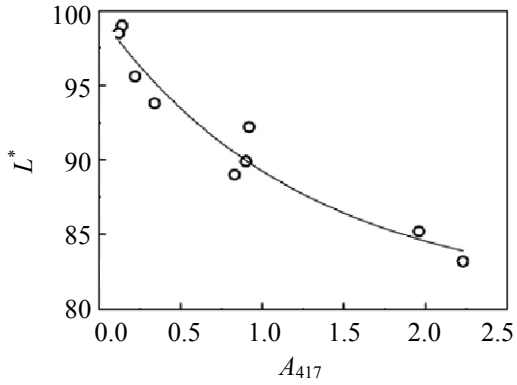

Fig. 14. Dependence of the lightness L^* of olive and rapeseed oils on absorptivity A_{417}.

Comparison of the spectra of olive oils (Fig. 12) [14] and pigments (Fig. 13) [15] shows that pigments contribute much in the oil colors, but this contribution considerably varies from sort to sort. The contribution of pigments in the color of rapeseed oils is not so essential.

The depth of olive oil color is most commonly measured by the absorptivity at 417 nm (A_{417}) which is the visible absorption maximum of chlorophyll (Fig. 13): The higher A_{417} the deeper the green oil color.

Table 2 lists the A_{417} values for the oils whose spectra are shown in Fig. 12. The tristimulus coordinates in the $L^*a^*b^*$ color space are shown in the same figure. Using these values we constructed the L^*–A_{417} dependence shown in Fig. 14. As seen from Table 2 and the oil color chart, the highest lightness (no color) is characteristic of rapeseed oils.

The L^*–A_{417} plot shows a scatter of points, which is probably explained by the fact that the color of different sorts of olive oils is also contributed by carotenoids absorbing at a wavelength close to that of chlorophylls (417 nm). Therewith, the difference in the concentration ratios of chlorophylls and carotenoids in different oils was not taken into account.

The scatter of points in the L^*–A_{417} plot is moderate, and, therefore, the L^* value can served as a quantitative basis for the evaluation of pigment concentrations in olive oils.

Evaluation of Human Skin Color

A dark color of human skin is associated with the presence of melanin, a dark brown pigment. The melanin concentration in skin is evaluated in terms of the so-called melanin index (MI) which is determined from reflection spectra [16]:

$$\mathrm{MI} = A_{640} - A_{670}.$$

Here A_{640} and A_{670} are the visible absorptivities of skin at 640 and 670 nm. As shown [16], the melanin index is proportional to the melanin concentration in skin.

Shriver and Parra [17] correlated the colors and MIs of skin of people belonging to different ethno-geographic groups (skin on forehead and underside of arm). For the colorimetric parameter of skin color the authors chose the lightness L^*. The measured MI and L^* values for several tens of volunteers are presented in Fig. 15.

Table 2. Absorptivities A_{417} in the visible spectra and tristimulus coordinates $L^*a^*b^*$ of olive and rapeseed oils

Sample no.	Oil code[a]	A_{417}	L^*	a^*	b^*
1	L EVOO (50%)	2.23	83.2	–12.3	110.5
2	F EVOO	0.92	92.2	–11.3	50.1
3	C (mixture)	0.22	95.6	–4.5	10.9
4	I EVOO	0.83	89.0	–11.6	74.0
5	H EVOO	0.90	89.9	–12.9	75.9
6	D mild	0.34	93.8	–5.1	20.4
7	K EVOO	1.96	85.2	–13.1	88.3
8	A rapeseed	0.14	99.0	–4.0	9.5
9	B rapeseed	0.12	98.5	–2.6	7.0

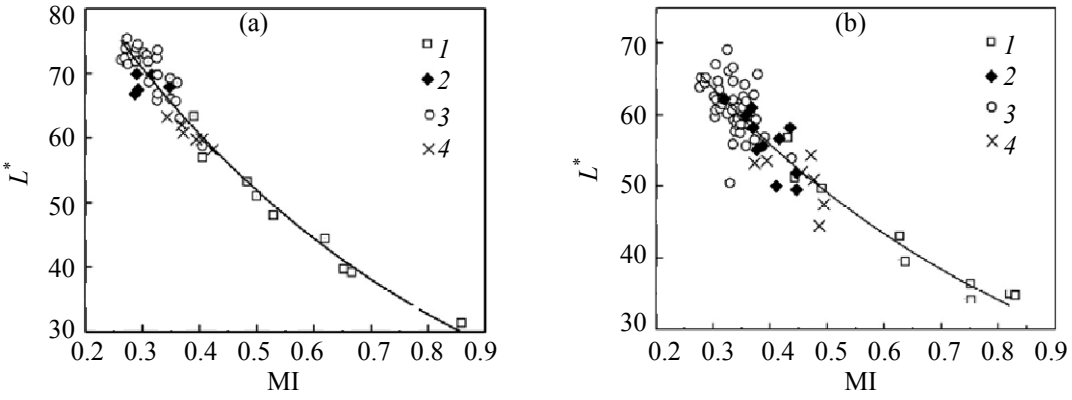

Fig. 15. Dependence of the lightness L^* of skin on (a) underside of arm and (b) forehead of people belonging to different ethnogeographic groups on melanin index (MI): (*1*) Afro-Americans, (*2*) East Asians, (*3*) Euro-Americans, and (*4*) South Asians.

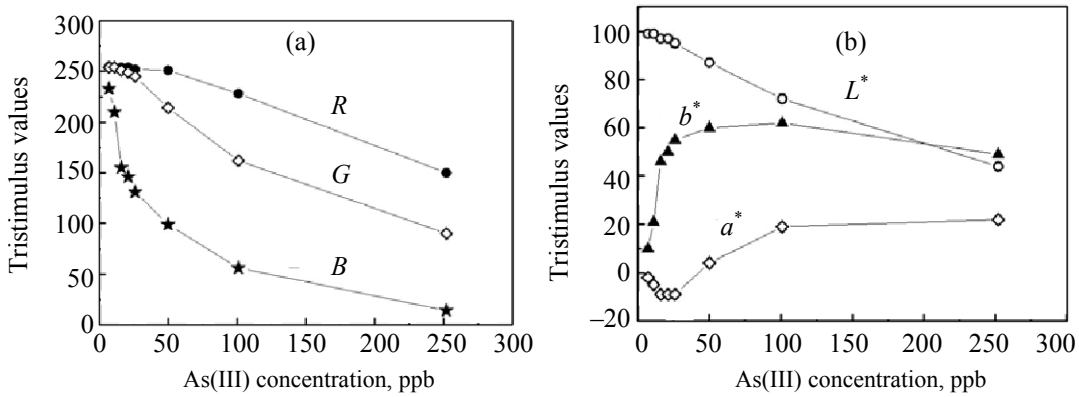

Fig. 16. Dependence of the (a) *RGB* and (b) $L^*a^*b^*$ tristimulus values on arsenic concentration.

Both dependences show a wide scatter of points. This is probably associated with the fact that the lightness of depends not only on its melanin level, but also on the levels of other pigments, as well as on some other factors, and the relative contributions of these factors vary from human to human. Note that the plots are steadily descending and can be fitted by an exponent.

Colorimetric Detection of Arsenic

Colorimetric detection of arsenic is based on the ability of arsenic compounds to be reduced by atomic hydrogen to form hydrogen arsenide which imparts a brown or yellow color to an indicator paper impregnated by mercury bromide (Gutzeit test). Ahuja [18] employed the Gutzeit test and Adobe Photoshop software for colorimetric analysis.

Digitalized color characteristics of indicator papers kept in standard test arsenic-containing solutions were used to construct concentration dependences of *RGB* color coordinates (Table 3 and Fig. 16).

The *RGB* coordinates were recalculated into $L^*a^*b^*$ coordinates. There data are also presented in Table 3, as well as in Fig. 16b. As seen from the figure, the concentration dependence of the lightness coordinate L^* is described by a steadily descending function. Thus, this dependence can be used as a calibration characteristic in the colorimetric measurements of arsenic concentrations in aqueous solutions.

Colorimetric Detection of Nitrite Ions

The method is based on a color reaction of diazotization of the end toluidine groups of foam polyurethane with nitrite ions in an acidic medium, followed by coupling of the polymeric diazonium cation with 3-hydroxy-7,8-benzo-1,2,3,4-tetrahydroquinoline [19]. The reaction product (a polymeric azo compound) can exist in two tautomeric forms: a red

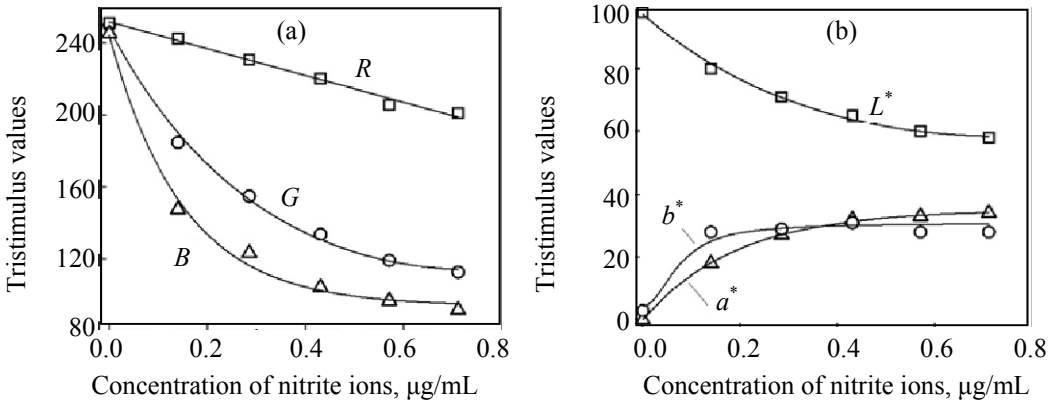

Fig. 17. Dependence of the (a) *RGB* and (b) $L^*a^*b^*$ tristimulus values on the concentration of nitrite ions for the color reaction product in the azoid form [19].

azoid form (470 nm) formed in an alkaline medium and a violet quinoid form (530 nm) formed after treatment of the polymeric azo compound with 5 M HCl.

Figure 17 shows the dependences of the *RGB* and $L^*a^*b^*$ coordinates of the test forms colored as a result of the described colored reactions on the concentration of nitrite ions in aqueous solutions [19].

As seen from Fig. 17b, the dependence of L^* on the concentration of nitrite ions is described, like with arsenic, by a steadily descending exponential function.

Consequently, this dependence can be used as a calibration characteristic in the colorimetric measurements of nitrite concentrations in aqueous solutions.

CONCLUSIONS

Automated instrumental methods for the detection and quantitation of chemical compounds in aqueous media by sensors of indicator test forms changing their color due to color reactions of chromogenic agents with analytes can be developed only if technologies for digitalization of the color characteristics of these test forms are available. The key stage of colorimetric research toward such methods is the choice of a color space coordinate uniquely related to the concentration of chromophores in an object to be studied.

Theoretical consideration shows that there are no simple analytical formulas relating any coordinates of such commonly accepted color spaces as (*RGB*), CIE (*XYZ*), CIE ($L^*a^*b^*$), CIE ($L^*C^*H^*$), (*HSB*), (*CMYK*) to the concentrations of colored substances or parameters of their optical spectra. Mathematically, this relation can be established by transformation by Eq. (1) and deduced numerically for each specific object. It should be emphasized that such transformation takes into account not only the visible spectrum of the object, but also the type of light source and such a subjective factor as human light perception. Clearly, experimental colorimetry data are extremely difficult to process under such conditions.

The situation could be much simplified, provided an empirical formula relating any color coordinate to chromophore concentration by a unique monotonic analytical function be available.

Using numerous published examples we showed that one of such coordinates is the color lightness L^* in the CIE $L^*a^*b^*$ space, which is one-to-one related to

Table 3. *RGB* and $L^*a^*b^*$ coordinates of indicator papers in the Gutzeit test at different arsenic concentrations in test solutions

Arsenic concentration, ppb	*R*	*G*	*B*	L^*	a^*	b^*
7	255	254	233	99	–2	10
11	254	254	210	99	–5	21
16	254	251	155	97	–9	46
21	254	249	146	97	–9	50
26	252	245	131	95	–9	55
50	251	214	99	87	4	60
101	228	162	56	72	19	62
252	150	90	14	44	22	49

the chromophore concentration in a colored substance. In all the cases we considered in the present paper the dependence of L^* on the analyte concentration C is described by a steadily descending exponential function. The resulting data point to the feasibility of the $L^*(C)$ dependence to instrumental processing of colorimetry data for measuring chromophore concentrations in indicator test forms and solutions.

REFERENCES

1. Zolotov, Yu.A., Ivanov, V.M., and Amelin, V.G., *Khimicheskie test-metody analiza* (Chemical Test Methods of Analysis), Moscow: Editorial URSS, 2002.
2. Kumpanenko, I.V., Roshchin, A.V., Marchenko, D.Yu., Khalfin, T.M., Ostrovskaya, V.M., Bloshenko, A.V., and Usin, V.V., *Khim. Fiz*., 2012, no. 10, pp. 52–65.
3. Sviridova, O.A., Dmitrienko, S.G., Senyavin, V.M., and Badakova, S.A., *Vestn. Mosk. Univ., Ser. 2: Khim*., 2002, vol. 43, no. 3, pp. 150–154.
4. *http://www.loveinfographics.com/categories/food-and-drink-infographics/the-many-colours-of-beer-infographic.*
5. *http://methodbrewery.com/srm.php.*
6. *http://www.franklinbrew.org/wp/?page_id=144.*
7. *http://beer.wikia.com/wiki/Standard_Reference_Method*.
8. *http://www.bjcp.org/colorguide.php*.
9. Smedley, S.M., *J. Inst. Brew*., 1995, vol. 101, p. 195.
10. Mazza, M., *Final Report. Department of Primary Industries, Future Farming Systems Research Division*, Irymple, Victoria, Australia, 2010, p. 34; *http://www.gwrdc.com.au/webdata/resources/project/DPI_05-01.pdf.*
11. Birse, M.J., *Ph.D Thesis*, Univ. of Adelaide, Australia, 2007, pp. 93, 106, *http://digital.library.adelaide.edu.au/dspace/bitstream/2440/42834/1/02whole.pdf* .
12. Giusti, M.M. and Wrolstad, R.E., *Current Protocols in Food Analytical Chemistry*, New York: Wiley, 2001, unit F1.2, p. 1, *http://www.nshtvn.org/ebook/molbio/Current%20Protocols/CPFAC/faf0102.pdf* .
13. Gordon, B., *Wine Color Analysis Using the Evolution Array UV-Visible Spectrophotometer, http://www.ana¬li¬ticaweb.com.br/newsletter/09/51852_UV_WineColor.pdf.*
14. Claverie, M. and Johnson, J.E., *The Determination of Extra Virgin Olive Oil from other Oils by Visible Spectroscopy*, Microspectral Anal., April 1, 2011. *http://www.microspectralasis.com/TechnicalDown¬loads/MSA%20White%20Paper% 20-Olive%20Oil%20%28REV%29.pdf.*
15. Lichtenthaler, H.K. and Buschmann, *Current Protocols in Food Analytical Chemistry*, New York: Wiley, 2001, unit F4.3, *http://www.nshtvn.org/ebook/molbio/Current%20Protocols/CPFAC/faf0403.pdf* .
16. Ohshima, H, Oyobikawa, M, Tada, A., et al., *Skin Res Technol*., 2009, no. 15, issue 4, p. 496.
17. Shriver, M.D. and Parra, E.J., *Am. J. Phys. Anthropol*., 2000, vol. 112, p. 17.
18. Ahuja, S., *Arsenic Contamination of Ground Water: Mechanism, Analysis and Remediation*, Hoboken, NJ: Wiley, 2008, p. 163, *http://books.google.ru/books?id=BiUJgDK3KnQC&pg=PA165&hl=ru&source=gbs_selected_pages&cad=3#v=onepage&q&f=false*.
19. Apyari,V.V., Dmitrienko, S.G., and Zolotov, Yu.A., *Vestn. Mosk. Univ. Ser. 2: Khim*., 2011, vol. 52, no. 1, p. 36.